A study on the simulation of blast actions on a monument structure

P. Vannucci, F. Masi, Ioannis Stefanou

A study on the simulation of blast actions on a monumental structure

P. Vannucci*[1], F. Masi[2,3], and I. Stefanou[3]

[1]LMV, Laboratoire de Mathématiques de Versailles - UMR8100 CNRS & UVSQ.
University Paris-Saclay, Versailles (F)

[2]Department of Industrial Engineering, University of Florence (I).

[3]Laboratoire Navier - UMR8205, CNRS, ENPC & IFSTTAR.
Université Paris-Est, Marne La Vallée (F)

February 1, 2017

Abstract

A strategy suited for the calculation of the blast actions on a monumental structure is presented in this paper; in particular, three different models are compared: JWL, CONWEP and TM5-1300. A procedure based upon new precise interpolations of the experimental data is detailed and a comparison of the above models is done on a case study referring to a typical monumental structure.

Key words: blast actions, fast dynamics, architectural monuments

1 Introduction

Architectural monuments of the past, as symbols of a cultural heritage proper to a nation, to a civilization or to a religion, have been unfortunately too often the objects of violences and iconoclastic destructions; the examples of the Cathedral of Reims in 1914, the Buddha statues of Bamyan in 2001 and the more recent destructions at Palmyra in 2015 and 2016 are just some few recent examples of that.

The present international situation has brought to the attention of people and governments the threat on highly representative monuments, that can be today the target of destructive bomb attacks. It is hence relevant to consider the mechanical problem of the effects of a blast on a monumental structure, which is the objective of this paper.

Rather surprisingly, literature is really poor about the studies on blast effects on monuments. The most part of papers concerning the effects of an explosion on a civil structure

*Corresponding author: Paolo Vannucci. LMV, 45 Avenue des Etats-Unis. 78035 Versailles, France
E-mail: paolo.vannucci@uvsq.fr

regard reinforced concrete structures and usually the geometries considered are really simple, normally a squared building, [Remennikov, 2003], [Ngo et al., 2007], [Koccaz et al., 2008], [Draganic and Sigmund, 2012], in some cases bridges, e.g. [Birhane, 2009].

When dealing with monument structures, we are usually faced to a different situation: the geometry is complex, sometimes very articulated. So, examining problems of explosions in monuments is case-dependent: the structural organization of the building affects in a particular way its response to the blast shock wave and failure modes proper to the building can be activated. Moreover, the determination of the blast loads can be very difficult, for at least two reasons.

On one side, reflected waves are very difficult to be taken into account, due to the complexity of the geometry. Curved surfaces of vaults, domes, columns, choirs and so on reflect shock waves while columns and pillars diffract them in a so complicated manner that it is practically impossible to model them in a numerical simulation of the blast using empirical approaches. On the other side, even taking into account for the wind pressure is very difficult, for exactly the same reason, the complexity of the geometry. Empirical rules used to evaluate the wind pressure for a blast in the interior of a building cannot be used, because such rules refer to so simple geometries that they cannot represent in any way the real situation of a monument.

In this paper, we propose a detailed study of the modeling of the blast actions, and a case test is studied on a simple structure typical of some monuments, like a church or a palace gallery: a structure covered by a barrel vault. The paper is subdivided into six Sections: the first one, Sect. 2, is devoted to a general description of the mechanical effects of a blast (we do not consider in this paper thermal effects nor the projection of fragments). The JWL model, [Jones and Miller, 1948], [Wilkins, 1964], [Lee et al., 1968], is shortly recalled in Sect. 3, while Sect. 4 is devoted to the empirical models for the calculation of the blast overpressure. In Sect. 5 we propose a procedure for the evaluation of the blast overpressure, using precise interpolating functions of the experimental data contained in the report [USACE, 1990], while in Sect. 6 we give a brief account of the model CONWEP, [USACE, 1986]. Finally, a comparison of the three models is given in Sect. 7, in a case study representing schematically the interior of a possible monument. A last Sect. 8 giving the conclusions ends the paper.

2 The mechanical effects of a blast

An explosion is actually an extremely rapid and exothermal chemical reaction that lasts just few milliseconds. During detonation, hot gases, produced by this chemical reaction, expand quickly and, for the hot temperatures produced instantaneously, the air around the blast expands too. The result is a blast shock wave, characterized by a thin zone of air propagating spherically much faster than the sound speed, through which pressure is discontinuous.

The shock-wave, travelling along a solid surface, produces an almost instantaneous increase of the air pressure on the surface, that decreases very quickly to the ambient pressure; this is the so-called positive phase of the blast. Then, the pressure decreases further, below the ambient pressure and then increases again to the ambient pressure,

but in a longer time; this is the negative phase of the blast, see Fig. 1. The shock wave is the main mechanical effect of a blast on a structure, but not the only one: the hot gases, expanding, produce the so-called dynamic pressure, least in value with respect to the shock wave and propagating at a lesser speed, while the impinging shock wave can be reflected by solid surfaces and act again on other surfaces as reflected shock wave.

To better understand all the mechanics of a blast, let us first introduce some quantities, used in the following:

- W: explosive mass;
- $R = ||q - o||$: distance of a point q from the detonation point o;
- P_o: ambient pressure;
- P_s: overpressure due to the blast; it is the pressure in the air relative to P_o;
- P_{so}: side-on overpressure peak: the shock-wave peak pressure, relative to P_o, measured in the air at q;
- P_r: reflected overpressure: the pressure, relative to P_o, acting at a point q of a solid surface when hit orthogonally by a shock-wave;
- P_{ro}: peak value of P_r;
- $P_{r\alpha}$: peak value of the reflected overpressure at a point q of a solid surface atilt of the angle α on the direction of $q - o$;
- t_A: arrival time, i.e. the instant at which the shock-wave peak arrives at q, taking as $t = 0$ the instant of detonation; of course, t_A increases with R, but experimental evidence has shown that it decreases with W, i.e. the velocity of the shock-wave increases with the quantity of explosive;
- t_o: positive phase duration; this is the duration of the time interval, starting from t_A, during which $P_s \geq 0$; t_o increases with R;
- t_{o-}: negative phase duration; this is the duration of the time interval, starting from $t_A + t_o$, during which $P_s < 0$;
- Z: Hopkinson-Cranz scaled distance, [Karlos and Solomos, 2013], defined as,

$$Z = \frac{R}{W^{\frac{1}{3}}}; \tag{1}$$

- i_s: impulse of the shock-wave positive overpressure, defined as

$$i_s = \int_{t_A}^{t_A+t_o} P_s(q,t)\ dt; \tag{2}$$

- i_r: impulse of the shock-wave positive reflected overpressure, defined as

$$i_r = \int_{t_A}^{t_A+t_o} P_r(q,t)\ dt; \tag{3}$$

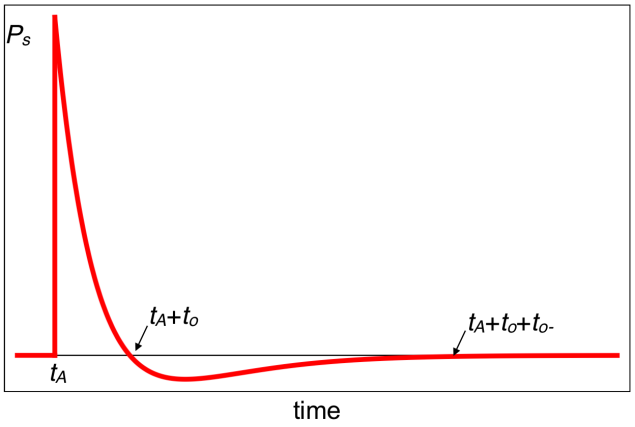

Figure 1: Scheme of the time variation of the pressure due to a blast.

- t_{rf}: fictitious duration of the positive phase of the blast, defined as

$$t_{rf} = \frac{2\ i_r}{P_{ro}}; \tag{4}$$

- $t_{Aw},\ t_{ow},\ t_{ow-}$: scaled durations, obtained dividing the respective durations by $W^{\frac{1}{3}}$;
- $i_{sw},\ i_{rw}$: scaled impulses, obtained dividing the respective impulses by $W^{\frac{1}{3}}$.

The overpressure P_s at a point q decreases with both the time $t > t_A$ and R. Generally, the time rate decrease is much greater than the space rate decrease: the blast overpressure is really like a very localized pressure wave that propagates at high speed and whose intensity decreases, like for any other wave, with the travelled distance.

Fig. 1 represents an ideal profile of the overpressure $P_s(q,t)$. When the shock wave arrives at q, after t_A from detonation, the pressure instantaneously increases, from the ambient pressure P_o to a peak P_{so}, which is a strong discontinuity.

For $t > t_A$ the overpressure decreases extremely fast, with an exponential rate, until time $t_A + t_o$, the end of the positive phase. After $t_A + t_o$ we have the negative phase: the pressure decreases with respect to P_o and then it returns to P_o after a time $t_{o-} > t_o$. Anyway, during the negative phase the decrease of the pressure is much lower, in absolute value, than the peak pressure of the positive phase, so usually the negative phase can be neglected for structural analyses, though it can be important in some particular cases, due to its duration, always much longer than the positive phase.

Generally, the activation time t_A decreases, for the same distance R, when the amount of explosive W increases, i.e. the velocity of the shock-wave increases. The peak value P_{so}, on its side, increases with W and decreases with R, while the time duration t_o does exactly the opposite, see Fig. 2.

The decrease of the pressure wave, i.e. the function $P_s(q,t)$, is an extremely rapid phenomenon; it can be modeled by the Friedlander's equation, [Karlos and Solomos, 2013]:

$$P_s(q,t) = P_{so}(q)\left(1 - \frac{t - t_A}{t_o}\right) e^{-b\frac{t-t_A}{t_o}}. \tag{5}$$

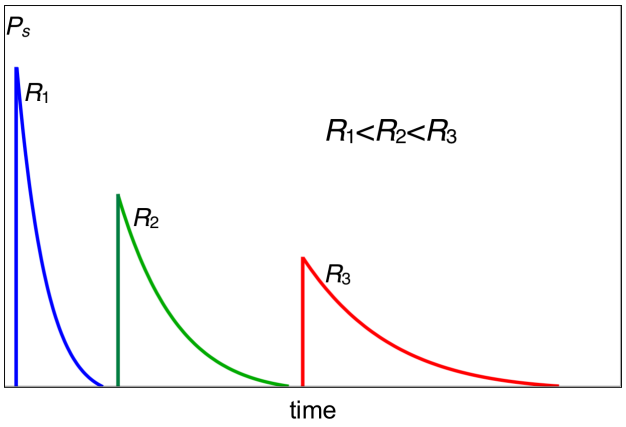

Figure 2: Influence of the distance R on the positive phase of a blast.

With this model, the impulse can be calculated analytically:

$$i_s(q,t) = P_{so}(q)\frac{t_o}{b^2}(b - 1 + e^{-b}). \tag{6}$$

This relation is useful for determining the coefficient b if i_s is known, e.g. from experimental data or with the method proposed below. The same rate decrease (5) is used also for the reflected overpressure, P_r.

P_r is the pressure that acts on a surface impinged by the incident overpressure P_s. The peak P_{ro} of P_r is normally much greater than P_{so} measured at the same point in the absence of any surface.

In fact, if we consider air as an ideal linear-elastic fluid, the air particles should bounce back freely from the surface, this giving a P_r equal to the double of the incident pressure. But normally, $P_{ro}/P_{so} > 2$ because a blast is actually a nonlinear shock phenomenon, where the reflection of the particles is hindered by subsequent air particles, with consequently a far higher reflected pressure.

A formula relating the values of P_{ro} and P_{so} for normal shocks is

$$P_{ro} = 2P_{so}\frac{4P_{so} + 7P_o}{P_{so} + 7P_o}, \tag{7}$$

The above equation indicates, on one side, that the ratio P_{ro}/P_{so} is not constant but depends upon P_{so} and, on the other side, that this ratio can vary between 2 and 8 or more. Of course, it is the value of P_{ro} to be used for structural design. The Friedlander's law is used also for describing the decrease of P_r.

Sometimes, the Friedlander's law is replaced by a simpler linear approximation, see Fig. 3. The fictitious positive duration time t_{rf} is then calculated imposing to preserve the same P_{ro} and i_r, which gives eq. (4).

The reflected pressure becomes, on its turn, an incident pressure for other surfaces, which of course complicates the situation: different incident waves can hit a surface besides the first one originated directly by detonation, all reflected by other surfaces, so giving a time history of the overpressure at a point that can have several successive peaks. However, normally the first peak is the highest one.

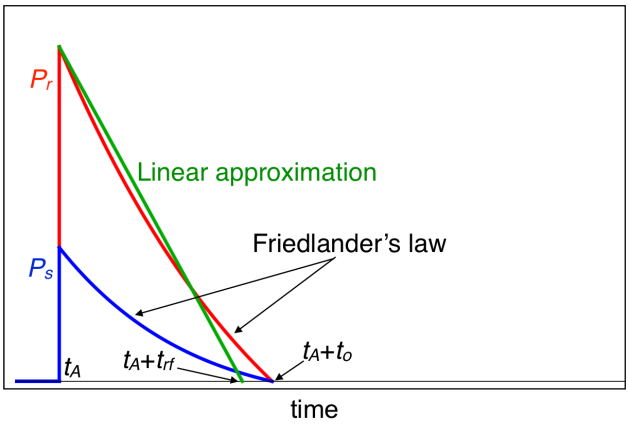

Figure 3: The Friedlander law.

Another phenomenon produced by a blast is the dynamic pressure; the air behind the front of the blast wave moves like a wind, but with a smaller velocity. This wind causes a *dynamic* or *drag* pressure Q, loading a surface for the whole duration of the wind produced by the blast. Its peak value Q_o is less than P_{so} and it is delayed with respect to t_A but Q has a much longer duration (up to $2 \div 3$ s) than t_o (some ms).

The blasts can be of different types:

- *free-air bursts*: detonation occurs in the air and the blast waves propagate spherically outwards and impinge first and directly onto the structure, without prior interaction with other obstacles or the ground;
- *air bursts*: detonation occurs still in the air but the overpressure wave arrives at the structure after having first interacted with the ground; a *Mach wave front* is created;
- *surface bursts*: detonation occurs almost at ground surface: the blast waves immediately interact locally with the ground and they propagate next hemispherically outwards and impinge onto the structure;
- *internal blasts*: detonation occurs inside a structure: blast waves propagates and interact with the different walls, reflected waves are generated and the effects of dynamic pressure due to gas expansion are amplified by the surrounding space.

In the case of explosions on monuments, we are concerned with surface blasts, i.e. with hemispherical overpressure waves. Surface blasts result in much greater shock overpressure than air-blasts, because of the ground effect, that reflects and amplifies the overpressure wave.

The case of internal blasts is also important in the study of monuments; nevertheless, in several cases an internal blast can be considered as an external one. This happens for buildings like churches or great halls, where the internal volume is so great to limit the effects of dynamic pressure and reflected waves.

The simulation of a blast can be conducted using different approaches, the most widely used being three: the JWL model, the CONWEP model and the TM5-1300 model. They are detailed in the following sections.

3 The JWL model

JWL stands for Jones, Wilkins and Lee, the authors of this model, [Jones and Miller, 1948], [Wilkins, 1964], [Lee et al., 1968]. Basically, JWL is a physically based model using the laws of thermodynamics to recover the physics of a chemical blast.

This model allows, in principle, to obtain a complete description of a blast phenomenon, i.e. including not only the propagation of the shock-wave in a medium, e.g. air, but also its reflection on solid surfaces and the expansion of the hot gases, i.e. the dynamic pressure. The JWL model is implemented in different commercial codes and its use needs the meshing not only of the structure but also of the air volume involved in the blast.

The JWL model gives the overpressure P_s as function of different parameters:

$$P_s = A\left(1 - \frac{\omega\ \rho}{R_1\rho_0}\right)\exp\left(-R_1\frac{\rho_0}{\rho}\right) + B\left(1 - \frac{\omega\ \rho}{R_2\rho_0}\right)\exp\left(-R_2\frac{\rho_0}{\rho}\right) + \omega\ \rho\ E_m. \quad (8)$$

In the above equation, $A,\ B,\ R_1,\ R_2$ and ω are parameters depending upon the explosive, along with ρ_0, its density, while ρ is the density of the detonation products and E_m is the internal energy per unit mass. In addition, detonation velocity v_D and the Chapman-Jouguet pressure p_{cj} need to be specified. All the parameters are derived by fitting experimental results.

The use of JWL model allows a rather precise and complete simulation of the blast phenomenon, but its drawback is the need of discretizing, finely, the charge and the fluid domain, that can be very large, besides the structure for the coupled structural analysis. Such multi-physics transient problems, with a strong coupling between fluid and structure dynamics, lead to numerical simulations that can be, in the case of a monument, very heavy, computationally speaking.

So this model, though in principle able to describe precisely the blast event and its mechanics, can be problematic to use in the case of monumental structures, where the fluid volume to discretize is very large.

4 Empirical models

Because of the drawbacks of the model JWL detailed hereon, empirical methods are more often used in the calculations. They offer a good balance between computing cost and precision. These models are based upon the results of experimental tests and model uniquely the effects of the blast, namely the pressure field.

With such models, the characteristic parameters of the explosive serve to calculate the overpressure shock-wave and its propagation speed. The wave propagates spherically from the detonation point o to the elements of the structure. The distance of o from any impact point q on a surface of the structure and the inclination of the perpendicular to the surface with respect to the vector $q - o$ are the only geometric parameters needed by the models.

In fact, these models consider just the incident wave, not the reflected ones, nor the dynamic pressure, that can be anyway calculated afterward. So, what is mainly lost with

empirical models is the possibility of taking into account for the set of reflected waves that impinge again the wall surfaces.

Nevertheless, the effect of the reflection of the shock-wave by the ground, in the case of a ground-explosion, is taken into account by specific laws, different from those modeling a free-air burst: the models for hemispherical blasts are not those for the spherical ones, the first ones giving higher values of the overpressure to take into account for the ground reflection and the formation of the so-called Mach stem.

This phenomenon is due to the reflection of the wave pressure by a surface. In general, the overpressure shock-wave due to an air detonation is produced by an incident wave, emanating from the explosive charge, and by a wave reflected, at least, by the ground. For small incident angles, up to about $40°$, the incident wave is ahead of the reflected wave produced by the surface and typical reflection occurs. However, for larger angles, coalescence between the incident and the reflected wave takes place, creating a Mach stem.

In ground explosions, the interaction between the ground and the blast wave takes place since the beginning, due to the closeness of the detonation point to the ground surface. Instead of the creation of a Mach front at a certain distance from the detonation point, the incident wave is reflected immediately by the ground. This wave coalescence can give much greater pressure values than the normal reflection.

If the ground were a rigid surface, the reflected pressure P_r would be twice that of a free-air burst. In practice, a part of the energy is absorbed by the creation of a crater, so P_r is less than the double of a free-air burst pressure, say $1.7 \div 1.8$ times.

The two most commonly used empirical models are based upon different but related studies of the U.S. Army Corps of Engineers (USACE): the document [USACE, 1986], containing the model CONWEP, and the Technical Manual TM5-1300, [USACE, 1990], completed by successive documents, [USACE, 2008]. The Joint Research Center of the European Union has produced in 2013 a Technical Report, [Karlos and Solomos, 2013], substantially referring to these two last documents and to another Technical Report of the U.S. Army, [Kingery and Bulmash, 1984]. In [Karlos and Solomos, 2013] all the empirical laws of [USACE, 1990] are reproduced using S. I. units.

It is worth recalling that [USACE, 1990] gives different rules for the calculation of the effects of a blast inside a building; all of them lead to an increase of the overpressure, but unfortunately they all refer to some simple geometrical situations, that practically never can represent, for dimensions and geometry, a typical internal volume of a monument, like a cathedral or a palace. That is why the use of these rules in such a context is quite problematic.

We give below a short description of these two models, but before we need to introduce the empirical laws used to calculate the overpressure peak P_{so} and other technical parameters.

4.1 Empirical laws for P_{so}

In the literature, there are several empirical laws for the prediction of P_{so}, all of them expressing it as function of the scaled distance Z, eq. (1). The most well known are (R in m, W in kg, P_{so} in MPa for all the formulas):

- *the Kinney-Graham formula* for spherical explosions, [Kinney and Graham, 1985]:

$$P_{so} = P_o \frac{808\left[1+\left(\frac{Z}{4.5}\right)^2\right]}{\sqrt{\left[1+\left(\frac{Z}{0.048}\right)^2\right]\left[1+\left(\frac{Z}{0.32}\right)^2\right]\left[1+\left(\frac{Z}{1.35}\right)^2\right]}}; \tag{9}$$

- *the Brode formula*, valid for spherical blasts too, [Brode, 1955]:

$$P_{so} = \begin{cases} \dfrac{0.67}{Z^3} + 0.1, & \text{for } P_{so} > 1\ MPa, \\ \dfrac{0.0975}{Z} + \dfrac{0.1455}{Z^2} + \dfrac{0.585}{Z^3} - 0.0019, & \text{for } P_{so} < 1\ MPa; \end{cases} \tag{10}$$

- *the Newark-Hansen formula* for hemispherical blasts, [Newmark and Hansen, 1961]:

$$P_{so} = \frac{678400}{Z^3} + \frac{2941}{Z^{\frac{3}{2}}}; \tag{11}$$

- *the Mills formula* for spherical explosions, [Mills, 1987]:

$$P_{so} = \frac{1.772}{Z^3} - \frac{0.114}{Z^2} + \frac{0.108}{Z}. \tag{12}$$

However, the most widely used method for blast parameters evaluation is based upon the experimental data of Kingery and Bulmash, [Kingery and Bulmash, 1984]. Such data concern both the cases of spherical and hemispherical explosions and most important they provide the data not only for the incident pressure peak P_{so}, but also for the reflected one, P_{ro}, which is by far most interesting for design purposes.

In Fig. 4 we show the value of P_{so} as predicted by the above models and by the Kingery and Bulmash experiments, whose data have been fitted, for both the cases of spherical and hemispherical blasts.

One can observe that the hemispherical case gives always higher values of P_{so} than the spherical one, for the two curves of Kingery and Bulmash, and that at small scaled distances, the predictions of the models of Brode, Newmark and Mills substantially deviates from those of Kingery and Bulmash. This is mainly due to the fact that the three mentioned models have been proposed for predicting the effects of nuclear blasts, not of a conventional explosive. On its side, the Kinney curve gives rather satisfactory predictions, i.e. similar to those of Kingery and Bulmash, for all the scaled distance range.

The experimental data of Kingery and Bulmash are represented in Fig. 5, uniquely for the positive phase of a blast, the most important one; such curves have been obtained by interpolating experimental values. The diagrams are referred to the explosion of 1 kg of TNT and concern a distance range from 0.5 to 40 m. As they are given as functions of Z, it is easy to adapt such data also to other cases, by multiplying by $W^{\frac{1}{3}}$ the value of the scaled parameters, except for pressure and velocity.

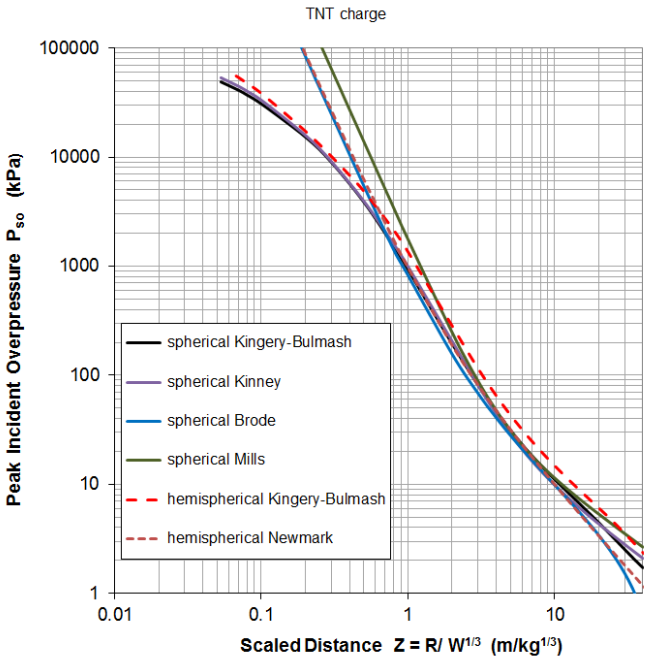

Figure 4: Comparison of P_{so} for different blast models (from [Karlos and Solomos, 2013]).

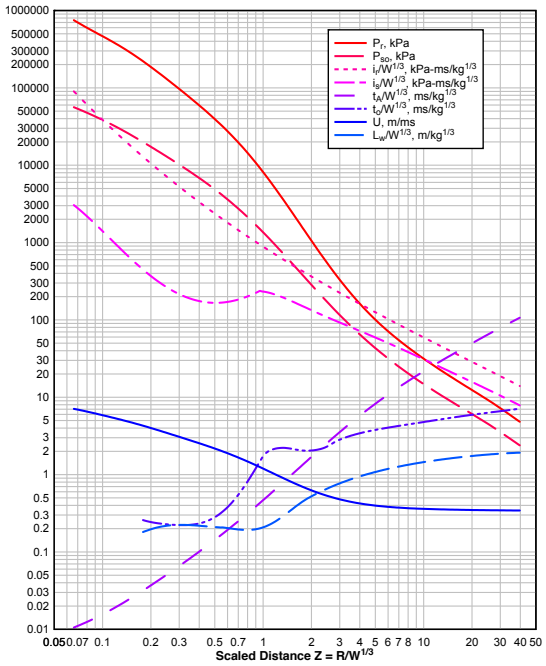

Figure 5: Blast parameters for the positive phase of a hemispherical blast, according to Kingery and Bulmash (from [Karlos and Solomos, 2013]).

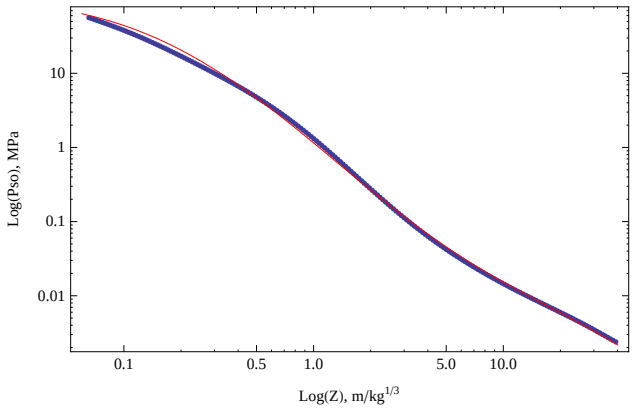

Figure 6: Comparison of experimental and fitted values of P_{so}.

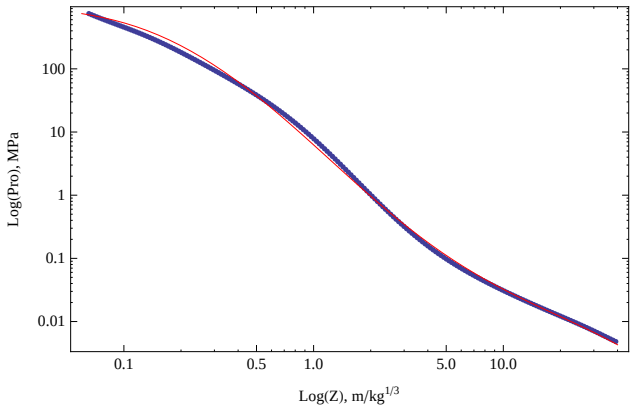

Figure 7: Comparison of experimental and fitted values of P_{ro}.

4.2 Interpolation of the Kingery-Bulmash data

In order to have precise analytical expressions of the diagrams of Fig. 5, we interpolated them and we give below the results for the different blast parameters of interest. The results are referred to the case of a hemispherical blast, the one of concern in our case. For each parameter, we give the analytical interpolating formula and a diagram comparing the experimental data, in blue, and the interpolating curve, in thin red. Among the parameters of Fig. 5, we have not interpolated the incident impulse i_s, the shock wave speed, U, and the blast wavelength, L_w, because they are not necessary in the following. The interpolating functions are:

- incident pressure P_{so}:

$$P_{so} = \exp\left(0.14 - 1.49 \ln Z - 0.08 \ln^2 Z - 0.62 \sin(\ln Z)\right)\left(1 + \frac{1}{2e^{10Z}}\right); \qquad (13)$$

- reflected pressure P_{ro}:

$$P_{ro} = \exp\left(1.83 - 1.77 \ln Z - 0.1 \ln^2 Z - 0.94 \sin(\ln Z)\right)\left(1 + \frac{1}{2e^{10Z}}\right); \qquad (14)$$

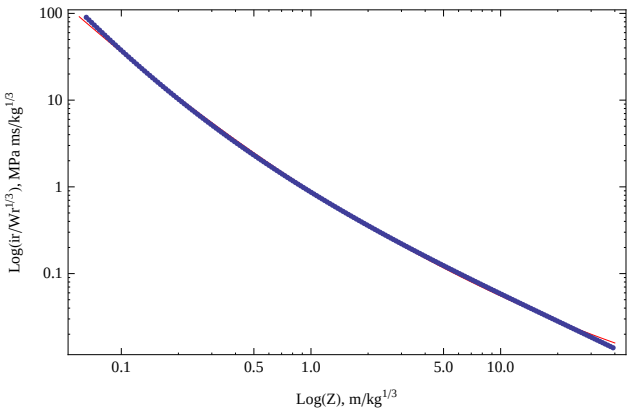

Figure 8: Comparison of experimental and fitted values of i_{rw}.

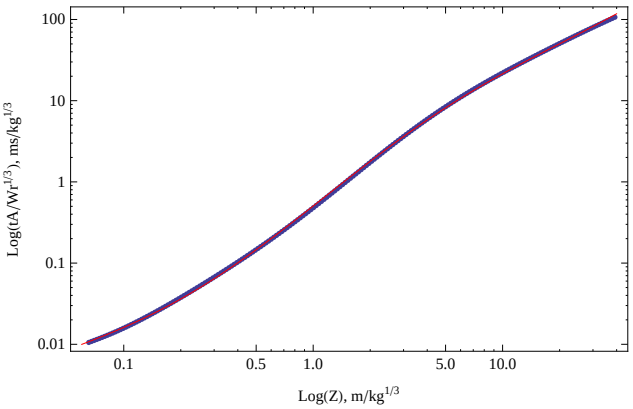

Figure 9: Comparison of experimental and fitted values of t_{Aw}.

- scaled reflected impulse i_{rw}:

$$i_{rw} = \exp\left(-0.11 - 1.41 \ln Z + 0.085 \ln^2 Z\right); \tag{15}$$

- scaled activation time t_{Aw}:

$$t_{Aw} = \exp\left(-0.685 + 1.429 \ln Z + 0.029 \ln^2 Z + 0.411 \sin(\ln Z)\right); \tag{16}$$

- scaled duration time t_{ow}:

$$\begin{aligned} t_{ow} = &\exp(-0.846 + 1.041 Z + 0.408 \ln Z - 1.105 \ln^2 Z - \\ &0.295 \ln^3 Z + 0.143 \ln^4 Z - 0.054 \ln^5 Z). \end{aligned} \tag{17}$$

4.3 Influence of the type of explosive

The experimental data and formulae for the blasts are always referred to TNT, used as reference explosive. To assess the effects of a blast produced by another explosive, an

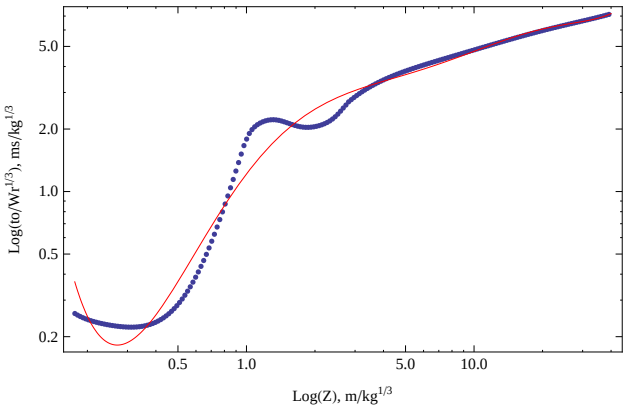

Figure 10: Comparison of experimental and fitted values of t_{ow}.

equivalent weight W of TNT is computed according to the following formula, that links the weight W_e of a chosen explosive to W using the ratio of the heat produced during detonation, [Karlos and Solomos, 2013]:

$$W = W_e \frac{H_e}{H_{TNT}}, \tag{18}$$

where H_e is the heat of detonation of the explosive and H_{TNT} is that of TNT. The values of the heat of detonation of some explosives are given in Tab. 1.

Table 1: Heat of detonation of different explosives (from [Karlos and Solomos, 2013]).

Type of explosive	**Heat of detonation** [MJ/kg]
TNT	$4.10 \div 4.55$
C4	5.86
RDX	$5.13 \div 6.19$
PETN	6.69
Pentolite 50/50	5.86
Nitroglycerin	6.30
Nitromethane	6.40
Nitrocellulose	10.60

5 Calculation of P_r on a surface using TM5-1300

5.1 Influence of the direction

The values of the incident and reflected pressures and impulses are intended for a normal shock, i.e. when the vector $q - o$ is orthogonal to the impinged surface in q. In such a case, the reflected pressure takes its maximum local value, that decreases when the shock is not orthogonal, i.e. when the vector $q - o$ forms an angle $\alpha > 0$ with the inward normal to the impinged surface.

The effect of the lack of orthogonality in the shock is taken into account introducing the *reflection coefficient* $c_{r\alpha}$, defined as

$$c_{r\alpha} = \frac{P_{r\alpha}}{P_{so}}, \tag{19}$$

where $P_{r\alpha}$ is the peak of the reflected pressure in q for a surface inclined of the angle α onto the direction of $q - o$. It is worth noticing that the reflection coefficient is defined as the ratio of the reflected inclined pressure $P_{r\alpha}$ with the incident pressure P_{so}, not P_{ro}.

The value of $c_{r\alpha}$ has been evaluated experimentally, and the results are shown in Fig. 11; this figure has been obtained from the parametrized curves given in [Karlos and Solomos, 2013]. To remark that $c_{r\alpha}$ depends not only upon α, but also upon P_{so}.

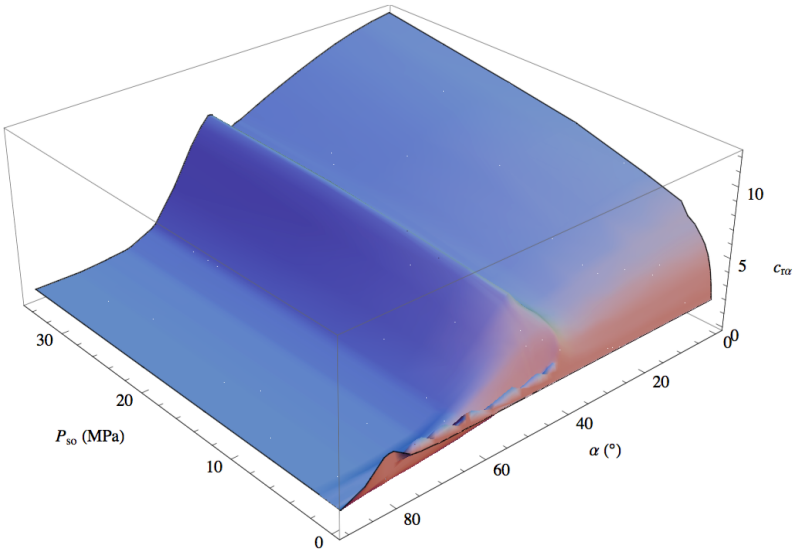

Figure 11: Surface representing $c_{r\alpha}(\alpha, P_{so})$.

In Fig. 12 we show also the interpolation of the empirical values of $i_{r\alpha w}$, still obtained from [Karlos and Solomos, 2013].

Looking at Fig. 11, one can see that $c_{r\alpha}$ is not a decreasing function of α, as it could be expected. Actually, for $\alpha >\sim 40°$, $c_{r\alpha}$ increases reaching a maximum and then it decreases again. This fact is attributed to the creation of the Mach stem cited above. For small values of P_{so} the behavior is more complicated, but this presumably could be the effect of imperfections in the experimental data.

5.2 P_r computing procedure

We detail in the following the sequence of the calculations to obtain, for a given blast, the time history of the reflected pressure $P_r(q, t)$ at the time t on a point q of a surface placed at a distance R from the detonation point o and whose inward normal forms an angle α with the vector $q - o$.

We make the following assumptions:

- the blast occurs at point o and is produced by a mass W_e of a given explosive;

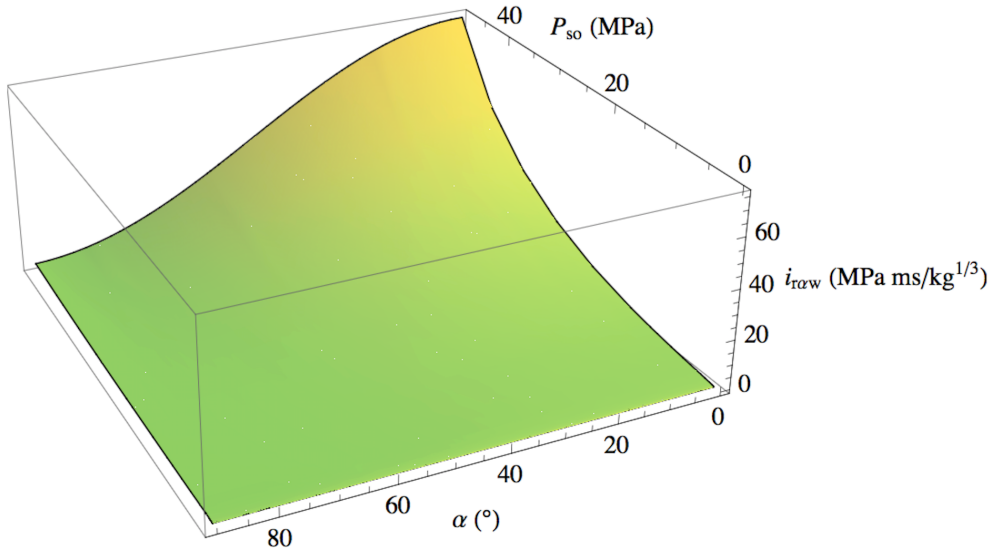

Figure 12: Surface representing $i_{r\alpha w}(\alpha, P_{so})$.

- the blast is hemispherical;
- the time rate decrease is of the same type for P_s and P_r and it is ruled by the Friedlander's equation;
- the calculation of the time history of P_s and P_r, as well as the impulse, is made pointwise;
- only the positive duration phase is considered; this assumption, usually done, is justified because of the much larger values of the positive pressures in comparison with the negative ones;
- reflected waves and dynamic pressure are ignored.

Then, the calculation sequence is the following one:

- a time duration t_{max} is fixed;
- t_{max} is subdivided into time intervals dt;
- the impinged surface is discretized into regular patches, whose centroids are points q;
- the equivalent mass of TNT W is calculated using eq. (18);
- then, for each point q we calculate:
  - the distance from the blast point: $R = ||q - o||$;
  - the inward normal $\mathbf{n}$ to the wall;
  - the angle α between $q - o$ and $\mathbf{n}$:

$$\cos\alpha = \frac{q-o}{R} \cdot \mathbf{n}; \tag{20}$$

  - the scaled distance Z, eq. (1);

– the normal incident pressure peak P_{so} using the fitted curve of Kingery-Bulmash for hemispherical blasts, eq. (13), Fig. 6;

– the normal reflected pressure peak P_{ro} using the fitted curve of Kingery-Bulmash for hemispherical blasts, eq. (14), Fig. 7;

– the ratio

$$c = \frac{P_{ro}}{P_{so}}; \tag{21}$$

– the angular coefficient $c_{r\alpha}$, eq. (19), by a linear interpolation of the experimental data represented by the surface in Fig. 11;

– the ratio

$$c_{r0} = \frac{P_{r0}}{P_{so}}, \tag{22}$$

i.e. $P_{r\alpha}$ for $\alpha = 0°$, still linearly interpolating the data of the surface in Fig. 11;

– the corrected value of $P_{r\alpha}$ as

$$P_{r\alpha} = c\frac{c_{r\alpha}}{c_{r0}}P_{so} = \frac{c_{r\alpha}}{c_{r0}}P_{ro}; \tag{23}$$

this correction is done to adapt the data of the interpolating surface in Fig. 11 to those of the Kingery-Bulmash fitted curves, Fig. 5, more conservative;

– the reduction coefficient

$$c_{red} = \frac{P_{r\alpha}}{P_{ro}} = \frac{c_{r\alpha}}{c_{r0}}; \tag{24}$$

– the positive normal scaled reflected impulse i_{rw} using the fitted curve of Kingery-Bulmash for hemispherical blasts, eq. (15), Fig. 8;

– the effective angular reflected impulse $i_{r\alpha}$ as

$$i_{r\alpha} = c_{red}\ i_{rw}\ W^{\frac{1}{3}}; \tag{25}$$

the value of $i_{r\alpha}$ is voluntarily *not* calculated interpolating the surface of experimental data, Fig. 12, like for $c_{r\alpha}$, because it has been observed, numerically, that the procedure described here is conservative;

– the scaled activation time t_{Aw} using the fitted curve of Kingery-Bulmash for hemispherical blasts, eq. (16), Fig. 9;

– the activation time t_A as

$$t_A = t_{Aw}W^{\frac{1}{3}}; \tag{26}$$

– the scaled positive duration time t_{ow} using the fitted curve of Kingery-Bulmash for hemispherical blasts, eq. (17), Fig. 10;

– the positive duration time t_o as

$$t_o = t_{ow}W^{\frac{1}{3}}; \tag{27}$$

- the fictitious positive duration time t_{rf}, eq. (4), as

$$t_{rf} = 2\frac{i_{r\alpha}}{P_{r\alpha}}; \tag{28}$$

- check on t_o: if $t_o < t_{rf}$ then put $t_o = 1.1\ t_{rf}$; this is done to avoid pathological situations, due to the fact that the Kingery-Bulmash curve for t_o does not cover low ranges of Z, see Fig. 5 and 10;
- solve numerically the equation

$$\frac{b - 1 + e^{-b}}{b^2} P_{r\alpha}\ t_o = i_{r\alpha} \tag{29}$$

  to determine the coefficient b of the Friedlander's equation.

- the time history of the pressure wave can now be calculated:
  - $t = n\ dt$;
  - $\forall q$:
    - if $t < t_A$ or $t > t_A + t_o$ then $P_r(q,t) = 0$;
    - else, use the Friedlander equation (5) with $P_{r\alpha}$ in place of P_{so} to evaluate $P_r(q,t)$;
  - iterate on t until $t > t_{max}$.

This sequence has been implemented in a program for the formal code *Mathematica* and applied to the case study presented in Sec. 7.

6 The CONWEP model

CONWEP is the acronym of CONventional Weapons Effects Programme, a study made by USACE, [USACE, 1986], for the simulation of the effects of a blast produced by conventional, i.e. not nuclear, explosives. The report [USACE, 1986] uses in many parts the same experimental results shown above, but not completely; in particular, a noticeable difference is the way in which the reflected pressure is calculated; in place of using the data represented in Fig. 12, and integrating the effect of the Mach stem, CONWEP makes use of the following law, using circular functions:

$$P_{r\alpha} = \begin{cases} P_{so}(1 + \cos\alpha - 2\cos^2\alpha) + P_{ro}\cos^2\alpha & \text{if } \cos\alpha \geq 0, \\ P_{so} \quad \text{if } \cos\alpha < 0. \end{cases} \tag{30}$$

The algorithm CONWEP is today implemented in different finite elements commercial codes, e.g. in *LS-DYNA*, *AUTODYN* or *ABAQUS*. In particular, in *ABAQUS*, the code we used for numerical simulations with CONWEP, the following assumptions are made:

- for each point q of the impinged walls, $P_{r\alpha}$ is calculated according to eq. (30);
- reflected waves are ignored;

- the dynamic pressure is neglected;
- the negative phase is taken into account;
- hemispherical blasts can be modeled.

So, the assumptions made by CONWEP are similar to those introduced in Sec. 5.2, except for the calculation of $P_{r\alpha}$ and the fact that in CONWEP the negative phase is considered too. That is why a comparison of the two methods is interesting, see the next Sec. 7.

A final, important remark is the fact that reflected waves and the dynamic pressure are ignored means that there is no difference between internal and external blasts: the only geometric parameters that matter are R and α, regardless of the surrounding geometry. For numerical simulations, this is interesting and important because it allows for modeling only a part of the building, the closest one to the detonation point, and to reasonably neglect the effects, at least in terms of applied pressures, of more distant parts. Therefore, only a part of the building can be modeled, saving in this way computing time.

7 Comparison of the models on a case study

Even though CONWEP and JWL models are implemented in some commercial finite element codes, this is not the same for the model TM5-1300. This is probably due to the fact that it is much easier to implement the dependence on the direction described by eq. (30) than the more accurate of TM5-1300, described in Fig. 11.

As said above, in the case of large buildings, like monuments, to make a complete non-linear fluid-solid simulation using the model JWL can be computationally expensive and unnecessary from an engineering point of view. This is why CONWEP is generally preferred.

The following comparison is hence made with the objective of evaluating the response of the model CONWEP, in comparison with both JWL and TM5-1300, and finally to calibrate its use in numerical simulations.

To evaluate the differences in the prediction of the blast parameters, and namely of the reflected pressure, between the three models, we consider an explosion in the interior of a building covered by a barrel vault, see Fig. 13. This is intended to simulate the typical structure of a monumental building, like a church or a palace gallery and so on, or also a domed structure. The dimensions used in this case are: width: 12 m, height of the walls: 12 m, radius of the vault: 6 m, total height: 18 m.

The explosive charge is composed by $W = 20$ kg of TNT, and detonates at the instant $t = 0$ at point $o = (0, 0)$. The problem is treated as a planar one, exception made for the JWL model, where a 3D approach is used.

The evaluation of $P_{r\alpha}$ is done in four different ways:

- using the JWL model, as implemented in *ANSYS Autodyn*; the results are indicated as JWL;

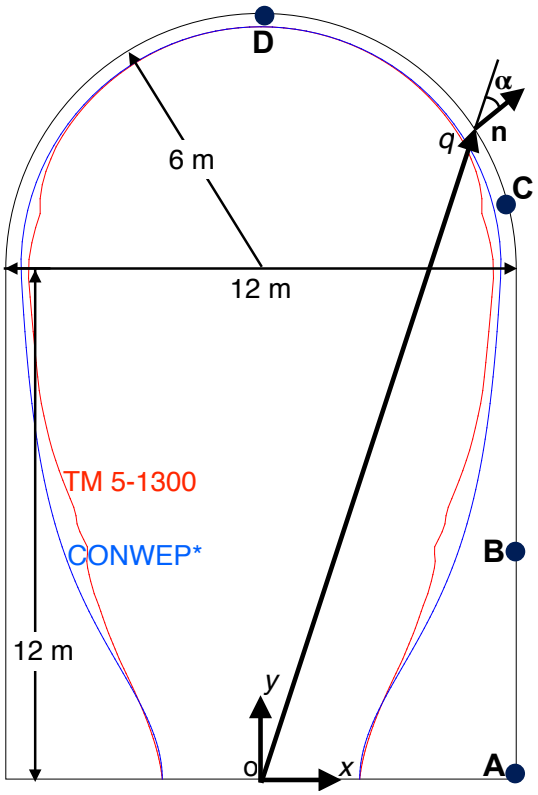

Figure 13: Case study: layout and $P_{r\alpha}$ distribution for the model TM5-1300 and CONWEP*.

- using the data of TM5-1300 and following modifications, as integrated into [Karlos and Solomos, 2013], and according to the calculation sequence presented in Sec. 5.2; the results are indicated as TM5-1300;
- using the data of TM5-1300 and following modifications, as integrated into [Karlos and Solomos, 2013], but evaluating the pressure $P_{r\alpha}$ according to eq. (30); the results are indicated as CONWEP*;
- applying the model CONWEP as implemented in *ABAQUS* to the above structure; the results are indicated as CONWEP.

The results TM5-1300 and CONWEP* are obtained using the program we have done in *Mathematica*.

7.1 The results from JWL

The analyses with the JWL model are run with *AUTODYN Hydrocode*, a code allowing good facilities in modeling the set of explosive, air domain and structure, where the equations of mass, momentum and energy conservation for inviscid flows are coupled with the dynamic equations of solid continua. A *Coupled Eulerian-Lagrangian* (CEL) method is used: explosive and surrounding air, as fluids, are modeled with an Eulerian frame, while solid walls are identified in a Lagrangian reference.

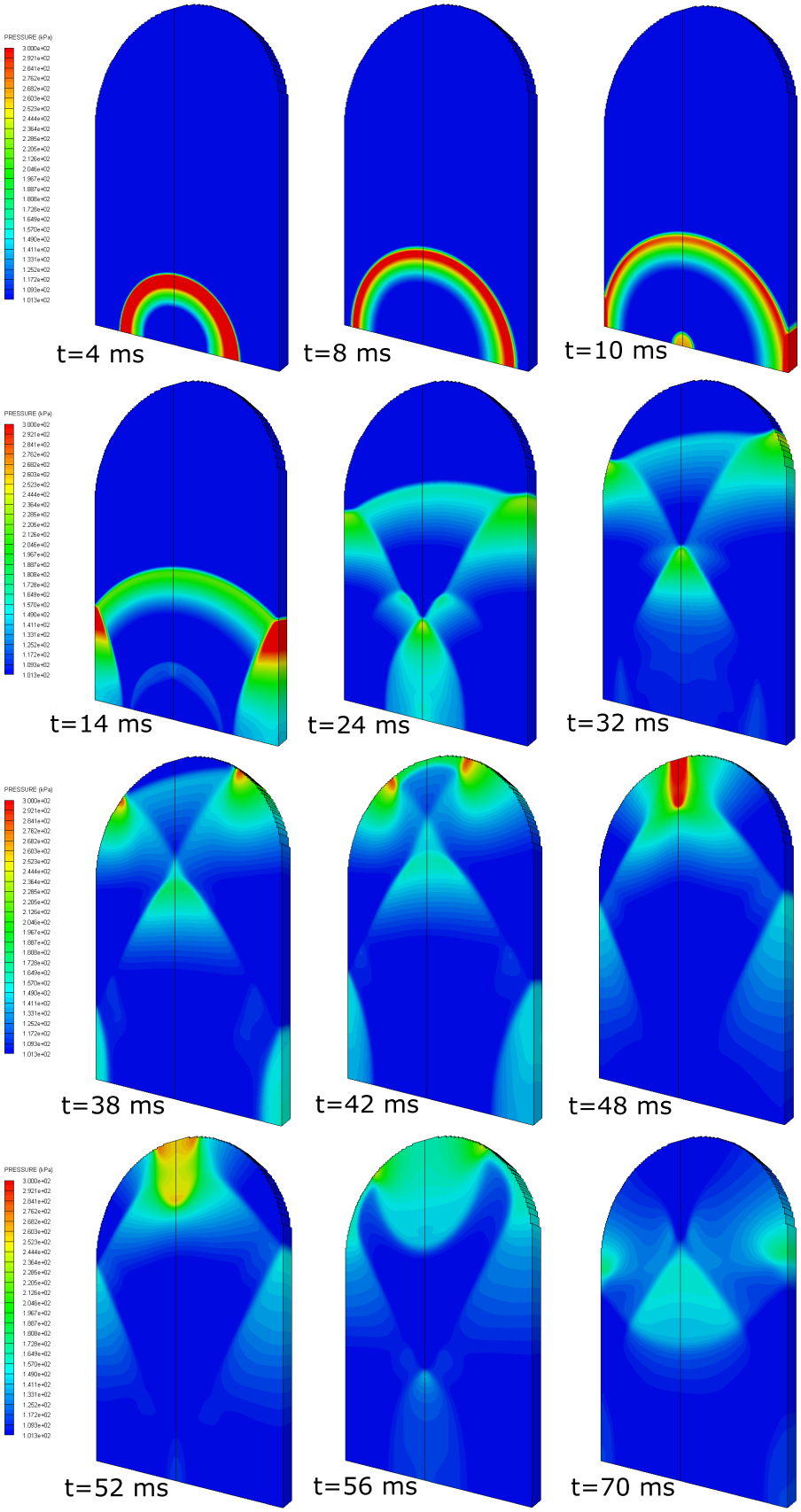

Figure 14: Evolution of the shock-wave as predicted by JWL.

The 3D geometrical model, taking advantage of symmetries, consists of a quarter of the entire domain. A volume having the transversal section like in Fig. 13 and a depth of 2 m is hence discretized. Ground and planes of symmetry are modeled as *reflecting planes* to prevent flow of material through them. The ending transversal surfaces are modeled as *transmitting planes*, i.e. boundary surfaces whereupon the gradients of velocity and stress are put to zero. This approach is used to simulate a far field solution at the boundary, it is only exact for outflow velocities higher than the speed of sound and is an approximation for lower velocities.

A preliminary study of the solution sensitivity to the cells size has been made studying the peak of the reflected pressure at point A of Fig. 13 for five different meshes. For each one of them, the dimensions of the volume elements discretizing the explosive charge and of the surface elements modeling the explosive-air and air-solid interfaces are decreased each time by a factor 1.5 starting from the coarsest mesh.

In Tab. 2 and in Fig. 15 we show the relative percent error, computed with respect to the finest discretization; it is apparent that it remains very small in all the cases. Attention needs to be paid when dealing with a CEL approach: more precisely, an almost equal size of the eulerian and lagrangian elements and an average grid size smaller than the thickness of the solid walls must be guaranteed. The simulations have been made with the mesh M2.

Table 2: Convergence study for different meshes.

Meshes	$\mathbf{M_1}$	$\mathbf{M_2}$	$\mathbf{M_3}$	$\mathbf{M_4}$	$\mathbf{M_5}$
Body sizing EXPLOSIVE [m]	0.0033	0.005	0.0075	0.01	0.015
Face sizing EXPLOSIVE-AIR / AIR-SOLID [m]	0.013	0.02	0.03	0.04	0.06
Relative error on P_{ro} at point A [%]	0.	0.018	0.059	0.106	0.274

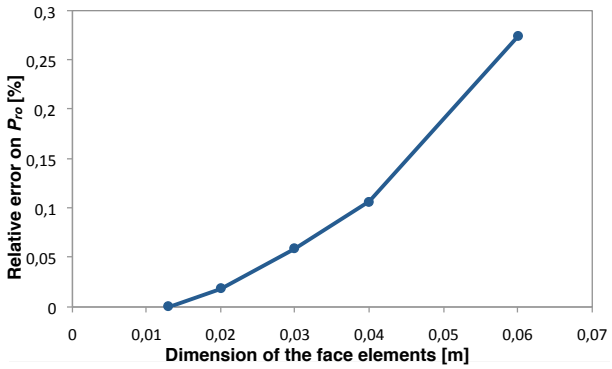

Figure 15: Convergence study for different meshes.

The results of the numerical simulation are presented in Fig. 14. It is apparent the formation not only of the principal, hemispheric shock-wave, but also fo the reflected ones, that produce the Mach stem, well visible in the photogram at $t = 14$ ms, at the bottom of the waves reflected by the vertical walls. At $t \sim 48$ ms, the incident and reflected waves focus just at the top of the vault, giving rise to a very high localized

pressure. Then, the reflected waves propagate downwards and upwards and decrease in intensity. Though not well visible in the figures, also the dynamic pressure is taken into account in this analysis.

The focusing of waves in the vault is not a surprising result and it is very similar to what observed by Rayleigh for acoustic waves in the study of the *whispering galleries*, [J. W. Strutton - Lord Rayleigh, 1910], [J. W. Strutton - Lord Rayleigh, 1914]: due to its geometry, the vault behaves like a concave (or converging) mirror for the shock waves, which has the tendency to collect the blast energy. As far as it concerns blasts, we can hence say that barrel vaults and domes have a dissatisfactory behavior.

What is clear, is the true complexity of the pressure dynamics, which cannot be predicted in advance and, most important, that is strongly depending upon the geometry and dimensions of the structure. Namely, the focalization described hereon takes place just because of the geometry of the vault and of its dimensions. To this purpose, we have also performed a simulation where the lowest part of the vertical walls, for a height of 7 m, are replaced by transmitting planes, to simulate the presence of openings, like in the case of an aisle. In such simulation, the peak at the key of the vault, produced by the focusing of the reflected waves, gives a sensibly smaller peak of the reflected pressure, reduced by a factor 2.72 with respect to that calculated in the above simulation, see Fig. 16, passing from 0.299 to 0.109 MPa.

It is not possible to recover such a complete description of the pressure history everywhere in the fluid domain, and on the walls, using the other empirical models. So it is interesting, for the comparison, to have the time-history of the pressure at a given point of the solid boundary. To this purpose, we give in Fig. 17 the diagram of the time variation of the reflected pressure P_r at four points of the boundary, indicated in Fig. 13 as points A, at the base of the vertical vault ($Z = 2.21$ m/kg$^{1/3}$), B, at 5.63 m from the base of the vertical wall ($Z = 3.03$ m/kg$^{1/3}$), C, at the springing of the vault ($Z = 5.40$ m/kg$^{1/3}$), and D, the key of the vault ($Z = 6.63$ m/kg$^{1/3}$).

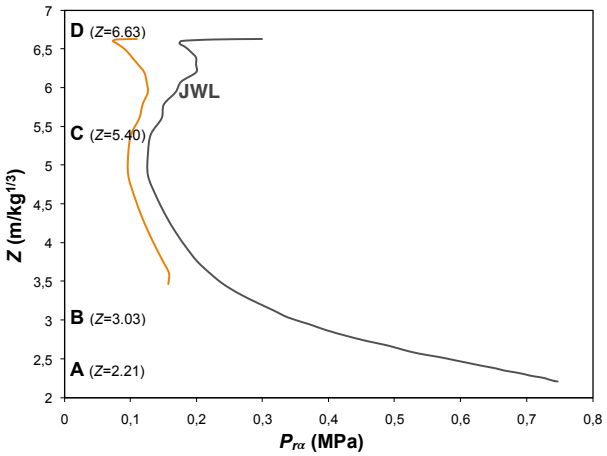

Figure 16: Comparison of $P_{r\alpha}$ as obtained by JWL for the two cases of complete vertical walls (black curve) and of openings until the height of 7 m (orange curve).

What is apparent is that the decay phase is not exactly as predicted by the Friedlander's law, and this because of the reflected waves, clearly visible on each diagram as secondary peaks of the curve. It is interesting to notice that the successive peaks are not necessarily

519 decreasing, which confirms the complexity of the interactions and dynamics of the reflected
520 waves.

Table 3: Simulation results for models TM5-1300 ($P_{r\alpha}1$) and CONWEP* ($P_{r\alpha}2$).

#	x [m]	y [m]	R [m]	Z $\left[\mathrm{m/kg^{1/3}}\right]$	α [°]	φ [°]	$P_{r\alpha}1$ [MPa]	$P_{r\alpha}2$ [MPa]	t_A [ms]	t_o [ms]	$t_A + t_o$ [ms]	b
1.	6.	0.	6.	2.21042	0.	90.	0.735886	0.735886	5.80172	7.20288	13.0046	5.08752
2.	6.	0.188558	6.00296	2.21151	1.8	90.	0.730865	0.73454	5.80677	7.20494	13.0117	5.08511
3.	6.	0.377488	6.01186	2.21479	3.6	90.	0.724034	0.730518	5.82196	7.2111	13.0331	5.07787
4.	6.	0.567167	6.02675	2.22027	5.4	90.	0.715496	0.723861	5.84739	7.22137	13.0688	5.06578
5.	6.	0.757976	6.04769	2.22799	7.2	90.	0.705346	0.714641	5.88323	7.23574	13.119	5.04882
6.	6.	0.950307	6.07479	2.23797	9.	90.	0.693531	0.702954	5.92974	7.25421	13.1839	5.02696
7.	6.	1.14456	6.10819	2.25028	10.8	90.	0.680578	0.688923	5.98724	7.27677	13.264	5.00017
8.	6.	1.34116	6.14807	2.26497	12.6	90.	0.666244	0.672692	6.05613	7.30342	13.3595	4.96838
9.	6.	1.54054	6.19462	2.28212	14.4	90.	0.650548	0.654428	6.1369	7.33415	13.4711	4.93155
10.	6.	1.74316	6.24809	2.30182	16.2	90.	0.633576	0.634314	6.23016	7.36895	13.5991	4.88962
11.	6.	1.94952	6.30877	2.32417	18.	90.	0.615423	0.612547	6.33659	7.40781	13.7444	4.84252
12.	6.	2.16013	6.377	2.34931	19.8	90.	0.596186	0.589338	6.45699	7.45072	13.9077	4.79019
13.	6.	2.37557	6.45316	2.37737	21.6	90.	0.575971	0.564906	6.59232	7.49766	14.09	4.73255
14.	6.	2.59643	6.5377	2.40851	23.4	90.	0.554887	0.539474	6.74364	7.54862	14.2923	4.66955
15.	6.	2.82339	6.6311	2.44292	25.2	90.	0.533405	0.513267	6.9122	7.60359	14.5158	4.60111
16.	6.	3.05715	6.73396	2.48081	27.	90.	0.514042	0.486509	7.09944	7.66255	14.762	4.52717
17.	6.	3.29853	6.84692	2.52243	28.8	90.	0.493955	0.459421	7.30699	7.7255	15.0325	4.44768
18.	6.	3.54839	6.97073	2.56804	30.6	90.	0.474135	0.432213	7.53675	7.79243	15.3292	4.36261
19.	6.	3.80772	7.10624	2.61796	32.4	90.	0.455844	0.405088	7.79088	7.86333	15.6542	4.27191
20.	6.	4.0776	7.25443	2.67256	34.2	90.	0.437248	0.378234	8.07188	7.93822	16.0101	4.17558
21.	6.	4.35926	7.41641	2.73223	36.	90.	0.41569	0.351825	8.38265	8.01711	16.3998	4.07363
22.	6.	4.65408	7.59345	2.79745	37.8	90.	0.398883	0.32602	8.72652	8.10004	16.8266	3.96608
23.	6.	4.96363	7.78702	2.86876	39.6	90.	0.384757	0.30096	9.10737	8.18708	17.2944	3.85299
24.	6.	5.28971	7.99882	2.94679	41.4	90.	0.383963	0.276765	9.52971	8.27832	17.808	3.73447
25.	6.	5.63438	8.23081	3.03226	43.2	90.	0.365806	0.253538	9.99883	8.3739	18.3727	3.61063
26.	6.	6.	8.48528	3.126	45.	90.	0.335087	0.231364	10.5209	8.47402	18.995	3.48166
27.	6.	6.38935	8.76492	3.22902	46.8	90.	0.319545	0.210307	11.1033	8.57895	19.6823	3.34776
28.	6.	6.80566	9.07288	3.34248	48.6	90.	0.285542	0.190412	11.7547	8.68909	20.4438	3.20923
29.	6.	7.25275	9.41289	3.46774	50.4	90.	0.251119	0.17171	12.4855	8.80492	21.2904	3.06641
30.	6.	7.73515	9.78941	3.60645	52.2	90.	0.218771	0.154212	13.3081	8.92713	22.2352	2.91969
31.	6.	8.25829	10.2078	3.76059	54.	90.	0.191973	0.137918	14.2375	9.05663	23.2942	2.76959
32.	6.	8.82873	10.6746	3.93255	55.8	90.	0.167226	0.122812	15.2922	9.19459	24.4868	2.61669
33.	6.	9.45449	11.1976	4.12525	57.6	90.	0.149989	0.108867	16.4948	9.34257	25.8374	2.46169
34.	6.	10.1454	11.7869	4.34232	59.4	90.	0.136025	0.096049	17.8733	9.50263	27.376	2.3054
35.	6.	10.914	12.4545	4.58828	61.2	90.	0.12172	0.0843127	19.463	9.67744	29.1405	2.1488
36.	6.	11.7757	13.2161	4.86887	63.	90.	0.106993	0.0736089	21.3087	9.87051	31.1792	1.99303
37.	5.96239	12.6707	14.0035	5.15893	58.3816	83.5816	0.115654	0.0703287	23.2485	10.0649	33.3134	1.85383
38.	5.82149	13.4527	14.6582	5.40014	52.5888	75.9888	0.129849	0.0692648	24.8837	10.2236	35.1073	1.75251
39.	5.60197	14.1489	15.2176	5.6062	47.4129	69.0129	0.0984861	0.0682742	26.2947	10.3576	36.6523	1.67499
40.	5.31949	14.7754	15.7038	5.78534	42.6467	62.4467	0.0854331	0.067366	27.5311	10.4731	38.0042	1.61363
41.	4.98432	15.3401	16.1296	5.94219	38.1727	56.1727	0.0772309	0.0665434	28.6206	10.5735	39.1941	1.56408
42.	4.60409	15.8474	16.5026	6.07963	33.9164	50.1164	0.0739119	0.0658065	29.5801	10.6611	40.2412	1.5236
43.	4.185	16.2995	16.8282	6.19956	29.8268	44.2268	0.0712106	0.0651542	30.4211	10.7372	41.1583	1.49037
44.	3.7324	16.6978	17.1098	6.30332	25.8672	38.4672	0.0690077	0.0645845	31.1512	10.8029	41.9541	1.46308
45.	3.2511	17.0429	17.3502	6.39186	22.0096	32.8096	0.0672195	0.0640955	31.776	10.8588	42.6347	1.44083
46.	2.74559	17.335	17.551	6.46586	18.2322	27.2322	0.0657855	0.0636853	32.2994	10.9054	43.2048	1.42292
47.	2.22013	17.5741	17.7138	6.52583	14.517	21.717	0.0646619	0.0633522	32.7244	10.9431	43.6675	1.40885
48.	1.67885	17.7603	17.8395	6.57213	10.8487	16.2487	0.0638169	0.0630946	33.053	10.9721	44.0252	1.39824
49.	1.12576	17.8934	17.9288	6.60503	7.21431	10.8143	0.063228	0.0629115	33.2868	10.9928	44.2796	1.39085
50.	0.564835	17.9734	17.9822	6.62471	3.60178	5.40178	0.0628804	0.0628019	33.4267	11.0051	44.4318	1.38648
51.	0.	18.	18.	6.63126	0.	0.	0.0627655	0.0627655	33.4732	11.0092	44.4824	1.38503

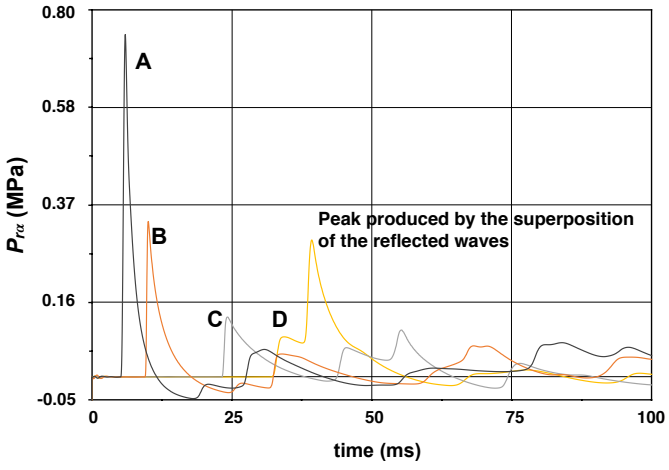

Figure 17: Time variation of $P_{r\alpha}$ at four points of the solid boundary, by JWL.

7.2 The results from TM5-1300 and CONWEP*

The spatial distributions of the maximum value of $P_{r\alpha}$ as given by TM5-1300 and CONWEP*, and calculated as specified above and in Sect. 5.2, are shown in Fig. 13. Such distributions are similar, though some differences exist:

- first of all, CONWEP* gives maximum values of $P_{r\alpha}$ that are almost always less or equal of those given by TM- 5-1300;
- the greatest differences appear for $0° < \alpha < 90°$; this can be explained by the fact that the angular variation taken by CONWEP does not take into account for the formation of the Mach stem;
- such occurrence happens really for $\alpha \simeq 40°$ and it is clearly indicated by the local increase of $P_{r\alpha}$ in the diagram of TM5-1300, that shows two humps: at midway of the vertical wall and at the springing of the vault where $\alpha \simeq 40°$ in both the cases; this fact can be of a great importance for vaulted structures, because an increase of $P_{r\alpha}$ in the zone between 0° and 30° can be very dangerous for the stability of the vault, that normally has on its back a filling with a material like rubble or gravel to improve the stability of the structure.

The numerical data of the simulations TM5-1300 and CONWEP* are shown in Tab. 3; φ is the angle formed by the normal $\mathbf{n}$ with the axis y, while b is the coefficient appearing in the Friedlander's law, eq. (5).

Observing the results concerning $P_{r\alpha}$ and t_o, we see clearly that the peak of the shock wave decreases with the distance R, passing from a maximum of 0.736 MPa for $R = 6$ m, to a minimum of 0.063 MPa for $R = 18$ m, while its time duration increases, passing from 7.2 ms to 11 ms.

In Fig. 18 we show the same curves of Fig. 17 but now obtained with the models TM5-1300, red curves, and CONWEP*, green curves. The red and green curves are distinct only for $\alpha \neq 90°$, for the way the values of CONWEP* are calculated.

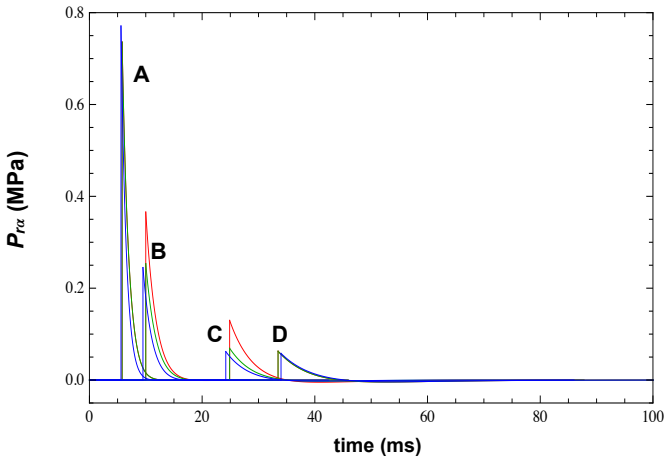

Figure 18: Time variation of $P_{r\alpha}$ at four points of the solid boundary, as predicted by TM5-1300 (red curves), CONWEP (blue curves) and CONWEP* (green curves).

Table 4: Simulation results for the CONWEP model.

#	x [m]	y [m]	R [m]	Z $\left[\mathrm{m/kg^{1/3}}\right]$	α [°]	φ [°]	$P_{r\alpha}$ [MPa]	t_A [MPa]	t_o [ms]	$t_A + t_o$ [ms]
1.	6.	.001	6.	2.21042	.0096	90.	.771063	5.5634	5.7978	11.3612
2.	6.	.003	6.	2.21042	.0287	90.	.732472	5.6309	5.7303	11.3612
3.	6.	.005	6.	2.21042	.0478	90.	.740335	5.3609	5.7303	11.3612
4.	6.	.007	6.	2.21042	.0669	90.	.672189	5.7658	5.6628	11.4286
5.	6.	.504	6.02113	2.21820	4.8040	90.	.686422	5.7658	5.7975	11.5633
6.	6.	1.1	6.1	2.24726	10.3941	90	.703576	5.7658	5.7975	11.5633
7.	6.	1.3	6.13922	2.26171	12.2313	90.	.68598	5.8333	5.7974	11.6307
8.	6.	1.5	6.18466	2.27845	14.0434	90.	.604788	6.0357	5.7297	11.7654
9.	6.	1.7	6.23618	2.29743	15.8272	90.	.628755	6.0357	5.8645	11.9002
10.	6.	1.9	6.29365	2.3186	17.5802	90.	.561932	6.2381	5.7969	12.0349
11.	6.	2.3	6.42573	2.36726	20.9841	90.	.588982	6.2381	5.999	12.237
12.	6.	2.7	6.57951	2.42391	24.24	90.	.533496	6.4404	5.9988	12.4392
13.	6.	2.9	6.66408	2.45507	25.8091	90.	.536047	6.5079	5.9986	12.5065
14.	6.	3.1	6.75352	2.48802	27.3378	90.	.515549	6.6428	6.0659	12.7086
15.	6.	3.3	6.84763	2.52269	28.8254	90.	.475994	6.8451	6.2004	13.0455
16.	6.	3.5	6.94622	2.55901	30.2718	90.	.442626	7.0474	6.2001	13.2475
17.	6.	3.7	7.04911	2.59692	31.6768	90.	.414128	7.2497	6.1999	13.4496
18.	6.	3.9	7.15612	2.63634	33.0406	90.	.389846	7.452	6.2671	13.7191
20.	6.	4.1	7.26705	2.6772	34.3635	90.	.369243	7.6543	6.4016	14.0559
21.	6.	4.3	7.38173	2.71945	35.646	90.	.351181	7.8565	6.6035	14.46
22.	6.	4.5	7.5	2.76302	36.8886	90.	.335817	8.0588	6.6707	14.7295
23.	6.	4.7	7.62168	2.80785	38.0921	90.	.322735	8.2611	6.8726	15.1336
24.	6.	4.9	7.74661	2.85388	39.2573	90.	.311071	8.4633	7.0744	15.5377
25.	6.	5.1	7.87464	2.90104	40.385	90.	.290647	8.7329	7.2089	15.9418
26.	6.	5.3	8.00562	2.9493	41.4763	90.	.273256	9.0026	7.2087	16.2112
27.	6.	5.5	8.13941	2.99858	42.532	90.	.266726	9.2048	7.4105	16.6153
28.	6.	5.7	8.27587	3.04886	43.5533	90.	.244744	9.5418	7.4777	17.0194
29.	6.	5.9	8.41487	3.10006	44.5411	90.	.233275	9.8113	7.5449	17.3562
30.	6.	6.1	8.55628	3.15216	45.4966	90.	.216588	10.1483	7.6119	17.7602
31.	6.	6.3	8.7	3.20511	46.4207	90.	.214245	10.3504	7.8139	18.1643
32.	6.	6.5	8.8459	3.25886	47.3146	90.	.194903	10.7548	7.8809	18.6357
33.	6.	6.7	8.99389	3.31338	48.1793	90.	.188719	11.0243	8.0155	19.0398
34.	6.	6.9	9.14385	3.36862	49.0158	90.	.178286	11.3612	8.0826	19.4438
35.	6.	7.1	9.2957	3.42456	49.8251	90.	.173488	11.6307	8.2172	19.8479
36.	6.	7.3	9.44934	3.48117	50.6083	90.	.160889	12.0349	8.217	20.2519
37.	6.	7.5	9.60469	3.53840	51.3662	90.	.157606	12.3044	8.3516	20.656
38.	6.	7.7	9.76166	3.59623	52.1	90.	.150868	12.6413	8.4187	21.06
39.	6.	7.9	9.92018	3.65463	52.8103	90.	.141494	13.0455	8.4859	21.5314
40.	6.	8.1	10.08018	3.71357	53.4983	90.	.133298	13.4496	8.5532	22.0028
41.	6.	8.3	10.24158	3.77303	54.1646	90.	.131731	13.7191	8.6877	22.4068
42.	6.	8.5	10.40433	3.83299	54.8102	90.	.124746	14, 1232	8.8223	22.9455
43.	6.	8.7	10.56835	3.89341	55.4358	90.	.121109	14.46	8.8895	23.3495
44.	6.	8.9	10.73359	3.95429	56.0422	90.	.115390	14.8642	8.8893	23.7535
45.	6.	9.1	10.9	4.01559	56.6302	90.	.107966	15.3357	8.8892	24.2249
46.	6.	9.3	11.06752	4.07731	57.2005	90.	.107626	15.6051	9.1585	24.7636
47.	6.	9.5	11.2361	4.13942	57.7536	90.	.103298	16.0092	9.2257	25.2349
48.	6.	9.7	11.4057	4.2019	58.2904	90.	.099298	16.4133	9.2256	25.6389
49.	6.	9.9	11.57627	4.26473	58.8114	90.	.095704	16.8174	9.2929	26.1103
50.	6.	10.1	11.74777	4.32791	59.3172	90.	.092426	17.2215	9.4275	26.649
51.	6.	10.3	11.92015	4.39142	59.8085	90.	.086272	17.7602	9.2928	27.053
52.	6.	10.5	12.09339	4.45524	60.2857	90.	.083664	18.1643	9.36	27.5243
53.	6.	10.7	12.26744	4.51936	60.7494	90.	.082638	18.501	9.562	28.063
54.	6.	10.9	12.44227	4.58377	61.2001	90.	.080329	18.9051	9.6292	28.5343
55.	6.	11.1	12.61784	4.64845	61.6382	90.	.075713	19.4438	9.5618	29.0056
56.	6.	11.3	12.79414	4.7134	62.0643	90.	.073825	19.8479	9.6964	29.5443
57.	6.	11.5	12.97112	4.7786	62.4789	90.	.072095	20.2519	9.7637	30.0156
58.	6.	11.7	13.14876	4.84405	62.8822	90.	.070498	20.656	9.8983	30.5543
59.	6.	11.9	13.32704	4.90972	63.2748	90.	.067946	21.1273	9.8983	31.0256
60.	5.99832	12.10025	13.5054	4.97543	63.6638	90.	.064633	21.6661	9.8981	31.5642
61.	5.99163	12.30062	13.68228	5.0406	62.1427	88.0809	.064329	22.0028	10.0328	32.0356
62.	5.95817	12.70015	14.02831	5.16807	59.1296	84.2299	.062510	22.9455	10.1	33.0455
64.	5.85816	12.79302	14.07051	5.38362	63.5136	88.0843	.062294	24.2249	10.2346	34.4595
65.	5.69932	13.8729	14.99799	5.52531	50.2785	72.5782	.062214	25.4369	10.5038	35.9407
66.	5.48322	14.43397	15.44038	5.68828	45.9365	66.7023	.061377	26.6490	10.5036	37.1526
67.	5.21205	14.97060	15.85195	5.83991	41.6396	60.7994	.059801	27.8610	10.5708	38.4318
66.	4.88854	15.47738	16.23105	5.97957	37.3838	54.8758	.060474	28.8036	10.8402	39.6438
67.	4.09793	16.38143	16.88621	6.22093	28.9900	42.9962	.059756	30.6216	10.9073	41.5289
68.	3.47738	16.88854	17.24282	6.35231	23.4836	35.0786	.059435	31.6316	11.1092	42.7408
69.	2.43397	17.48322	17.65183	6.50299	15.3680	23.2520	.058859	32.8435	11.1765	44.0200
70.	1.29302	17.85816	17.90491	6.59623	7.4347	11.5324	.058495	33.6515	11.3111	44.9626
71.	.50299	17.93144	17.93850	6.6086	1.53009	.0318	.059572	33.7188	11.4458	45.1646
72.	.001	17.99832	17.99832	6.63064	.00319	.0456	.058515	34.0555	11.3784	45.4339

7.3 The results from CONWEP

The same case study has finally been implemented in *ABAQUS* in order to make a comparison also with the results given by the model CONWEP. The comparison, as already said, will serve to understand the quality of the predictions given by CONWEP and to calibrate its use.

The problem is still considered planar and the mesh consists of linear quadrilateral elements with an average size of 0.2 m and a thickness of 0.1 m.

The results obtained with this simulation are reported in Tab. 4, while the diagrams of the time variation of the reflected pressure P_r at the four points A, B, C and D of the boundary are still shown in Fig. 18.

Table 5: Comparison of the characteristic parameters evaluated at points A, B, C and D of Fig. 13 as calculated by JWL, TM5-1300, CONWEP* and CONWEP; R_1 =*JWL/TM5-1300*, R_2 =*JWL/CONWEP*, R_3 =*TM5-1300/CONWEP*.

	JWL	**TM5-1300**	**CONWEP***	**CONWEP**	$\mathbf{R_1}$	$\mathbf{R_2}$	$\mathbf{R_3}$
			$\mathbf{P}_{r\alpha}$ [MPa]				
A	0.746	0.736	0.736	0.771	1.01	0.97	0.95
B	0.339	0.366	0.253	0.245	0.93	0.72	1.49
C	0.131	0.130	0.070	0.062	1.01	2.11	2.10
D	0.299	0.063	0.063	0.058	4.75	5.15	1.09
			$\mathbf{t_A}$ [ms]				
A	5.9	5.8	5.8	5.6	1.02	1.05	1.03
B	10.1	10.0	10.0	9.5	1.01	1.06	1.05
C	24.3	24.9	24.9	24.2	0.97	1.00	1.03
D	39.3	33.5	33.5	34.0	1.17	1.15	0.98
			$\mathbf{t_o}$ [ms]				
A	5.7	7.2	7.2	5.8	0.81	0.98	1.24
B	7.7	8.4	8.4	7.5	0.92	1.03	1.12
C	13.9	10.2	10.2	10.2	1.36	1.36	1.00
D	16.9	11.0	11.0	11.4	1.53	1.48	0.96

7.4 Comparisons

In order to compare the results of the above simulations, something must be mentioned about the results from JWL. On one hand, the multiple reflections of the shock-wave, visible in Fig. 14, completely alter the time variation of P_r after the positive phase, that in some cases can be even difficult to be determined. On the other hand, the multiple reflections add together and can considerably increase the value of P_r. Nevertheless, it is still possible, at least for a part of the boundary surface, to focus on just the characteristic elements of the positive phase, namely $P_{r\alpha}$, t_A and t_o. Such a comparison, of course, is possible only if the peak $P_{r\alpha}$ has not yet been affected by other reflected shock-waves and if a positive phase is still clearly distinguishable, which depends again on the reflected waves.

To assess the results, we have chosen to consider the relevant physical parameters of the blast: $P_{r\alpha}$, t_A and t_o. We have compared them as evaluated at the four points A, B, C and D of Fig. 13; these values are summarized in Tab. 5.

In Fig. 19 we show a comparison of the results for the values of $P_{r\alpha}$ obtained with JWL, TM5-1300, CONWEP* and CONWEP. The latter ones, as already pointed out, use the

empirical data for computing P_r for $\alpha = 0$, but a different angular dependence from α, eq. (30).

It can be observed that the values given by CONWEP and the code *ABAQUS* are practically coincident with those calculated using the model CONWEP*, except some oscillations, to be imputed to the finite element approximation. Hence, on one side the computation of P_{ro} is practically the same for the three models, but what changes is the way the effect of the inclination α is taken into account. In particular, except the value $\alpha = 0$, where the three models give the same value of P_{ro}, for all the other values of α, CONWEP and CONWEP* underestimate the value of $P_{r\alpha}$ with respect to TM5-1300.

TM5-1300 and JWL give values that are comparable until point C; here, JWL diverges and gives values of $P_{r\alpha}$ that can be considerably greater. This is actually the effect of converging the reflected waves, that increases significantly the value of the overpressure. It is a local phenomenon, essentially depending upon the geometry and dimensions of the structure, as shown above. This same phenomenon is noticed also on the time variation of $P_{r\alpha}$ for point D in Fig. 17, where the peak due to the reflected waves is clearly visible.

It is worth noticing that, besides the convergence of the reflected waves starting from point C, JWL and TM5-1300 give not only comparable values of $P_{r\alpha}$, but also of its time variation. In Fig. 20 we show the time diagrams of JWL, reduced to the positive phases, presented together with those of TM5-1300. The curves are in a rather good agreement, apart from the peak on the curve of point D, due to reflected waves.

As far as it concerns the time durations, represented in Fig. 21, TM5-1300 and CONWEP* give, of course, the same values, while CONWEP underestimates slightly the durations for small values of Z. Nevertheless, these discrepancies are not significant. The diagrams in Figs. 19 and 21 explain the aforementioned slight differences, namely in the value of t_A, appearing in Fig. 18 between the curves obtained with CONWEP and those relative to TM5-1300 and CONWEP*.

For what concerns JWL, the curve of t_A is in a very good agreement with those of TM5-1300 and CONWEP until point C, where it diverges, once more due to wave reflection. The curve of $t_A + t_o$ has been obtained by interpolating the values estimated for points A, B, C and D for the duration t_o because, as mentioned above, it is not easy to determine the exact duration of the positive phase for all the points, due to the interaction of the reflected waves. Globally, the four models give values that are comparable, apart the zone of the wave reflections, where the values given by JWL diverge from those of the other models.

8 Conclusion

The results of the simple example treated above clearly show that the distribution of the pressures given by TM5-1300 is sensibly similar to that given by the more exact JWL model, apart from those zones where the interaction of the reflected waves alters the overpressure distribution. This phenomenon, as already explained, strongly depends upon the geometry and the dimensions of the structure and cannot be predicted *a priori*.

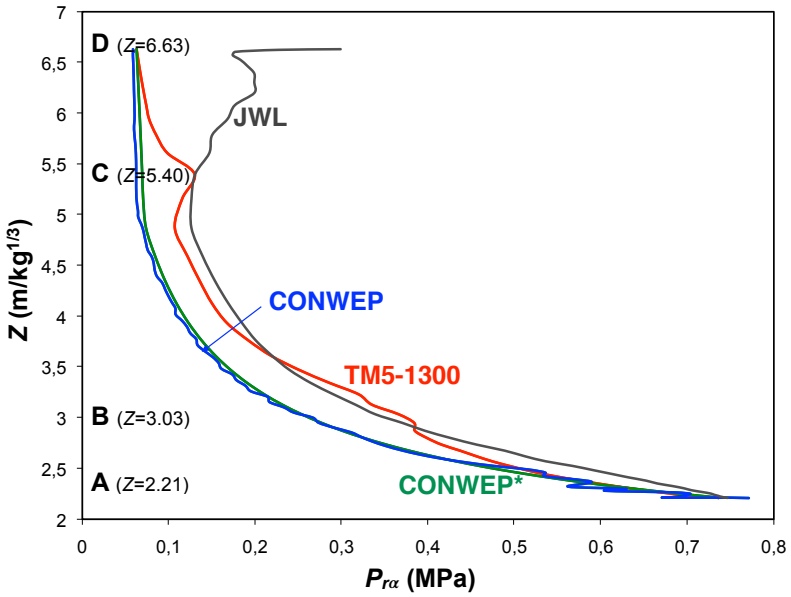

Figure 19: Comparison of $P_{r\alpha}$ as obtained by the four models.

Simulations done with the model JWL are hence the best way to predict the effects of an explosion on a monument. However, the use of JWL can be impractical, if not impossible, in real problems of large structures. The need of discretizing finely not only the structure but, even more, the explosive charge and the volume of air is an almost insurmountable obstacle for numerical simulations. Due to the great volume of the air and of the structure to be finely discretized, the size of the numerical problem becomes very heavy and impossible to treat in reasonable time.

That is why the use of empirical models, like TM5-1300 and CONWEP, can be very useful. If abstraction is made concerning the effect of reflected waves, the results of TM5-1300, though obtained neglecting the dynamic pressure, are close to those of JWL, incorporating it, which confirms that the dynamic pressure can be neglected in simulations.

The comparison made of CONWEP, TM5-1300 and JWL confirms what usually said in the literature: TM5-1300 is more accurate than CONWEP. Nevertheless, as mentioned above, it is this last model that normally is implemented in commercial finite element codes. That is why its use must be accurately considered, adopting a multiplying factor $p_f > 1$. Such a coefficient, affecting only the reflected pressure $P_{r\alpha}$ and not the other blast parameters, namely t_A and t_o, is needed to obtain values that are similar to those predicted by TM 5-1300 and JWL; it represents hence, on the average, the ratio between the value of $P_{r\alpha}$ given by JWL and that given by CONWEP. This coefficient must be chosen in function of the problem at hand, namely considering the characteristic dimensions of the building: as apparent from Fig. 19, p_f depends upon Z, hence upon R, and upon the angle α. For monuments of large dimensions, we can suggest a value in the interval $1.5 \div 2.5$, in order to take into account, though indirectly, of the effect of reflected waves.

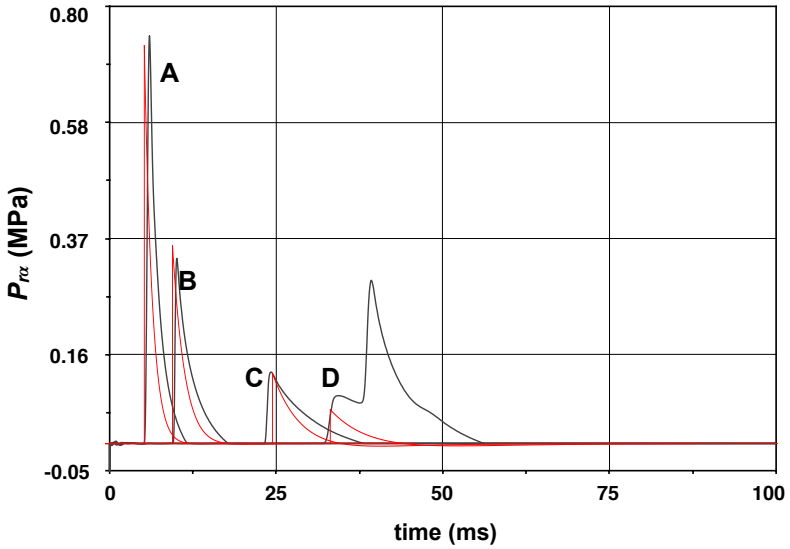

Figure 20: Comparison of the positive phases for points A, B, C and D as given by JWL (black) and TM5-1300 (red).

References

T. H. Birhane. Blast analysis of railway masonry bridges. Master's thesis, University of Minho, Portugal, 2009.

H. L. Brode. Numerical solution of spherical blast waves. *Journal of Applied Physics*, 26: 766, 1955.

H. Draganic and V. Sigmund. Blast loading on structures. *Technical Gazette (Croatia)*, 19:643–652, 2012.

J. W. Strutton - Lord Rayleigh. The problem of the whispering gallery. *Philosophical Magazine, Series 6*, 20:1001–1004, 1910.

J. W. Strutton - Lord Rayleigh. Further applications of Bessel's functions of high order to the whispering gallery and allied problems. *Philosophical Magazine, Series 6*, 27: 100–109, 1914.

H. Jones and A. R. Miller. The detonation of solid explosives. *Proc. Royal Soc. A*, 194: 480, 1948.

V. Karlos and G. Solomos. Calculation of Blast Loads for Application to Structural Components. Technical report, Joint Research Center of the European Commission, 2013.

C. N. Kingery and G. Bulmash. Technical report ARBRL-TR-02555: Air blast parameters from tnt spherical air burst and hemispherical burst. Technical report, U.S. Army Ballistic Research Laboratory, 1984.

G. F. Kinney and K. J. Graham. *Explosive Shocks in Air*. Springer, 1985.

Z. Koccaz, F. Sutcu, and N. Torunbalci. Architectural and structural design for blast

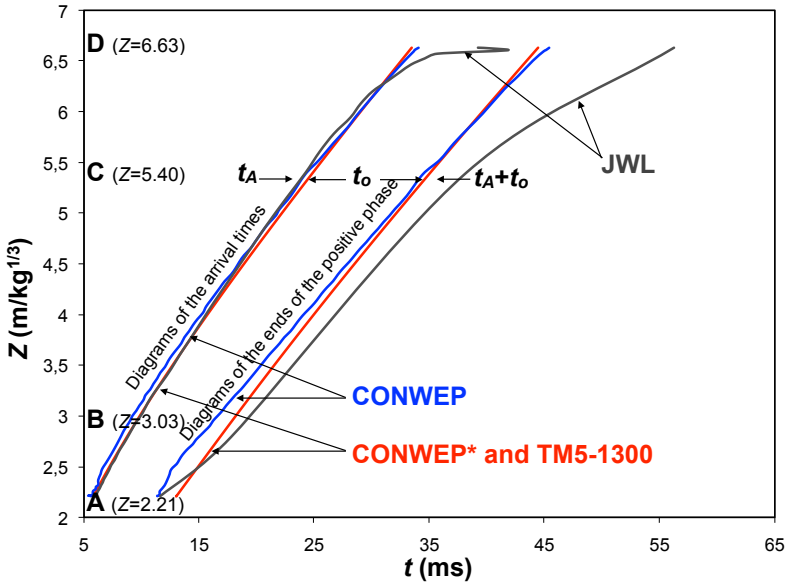

Figure 21: Comparison of the arrival time t_A and of the positive phase duration t_o as obtained by the four models.

resistant structures. In *Proc. of 14th World Conference on Earthquake Engineering*, Beijing, 2008.

E.L. Lee, H.C. Horning, and J.W. Kury. Adiabatic expansion of high explosives detonation products. Technical Report TID 4500 - UCRL 50422, Lawrence Livermore National Laboratory, 1968.

C. A. Mills. The design of concrete structures to resist explosions and weapon effects. In *Proceedings of the 1st Int. Conference on concrete for hazard protections*, Edinburgh, 1987.

N. M. Newmark and R. J. Hansen. Design of blast resistant structures. In Harris & Crede, editor, *Shock and Vibration Handbook*. McGraw-Hill, New York, 1961.

T. Ngo, P. Mendis, A. Gupta, and J. Ramsay. Blast loading and blast effects on structures - An overview. *Electronic Journal of Structural Engineering*, Special Issue: Loading on Structures:76–91, 2007.

A. M. Remennikov. A review of methods for predicting bomb effects on buildings. *J of Battlefield Techn*, 6:5–10, 2003.

USACE. TM 5-855-1: Design and Analysis of Hardened Structures to Conventional Weapons Effects. Technical report, U. S. Army, 1986.

USACE. TM 5-1300: Structures to Resist the Effects of Accidental Explosions. Technical report, U.S. Army, 1990.

USACE. UFC 3-340-02: Structures to Resist the Effects of Accidental Explosions. Technical report, U.S. Army, 2008.

M. L. Wilkins. The equation of state of PBX 9404 and LX 04-01. Technical Report UCRL - 7797, Lawrence Radiation Laboratory, 1964.